# Square arrays of vertically aligned nanoporous cylinders from a linear ABC triblock terpolymer

Karim Aissou, Muhammad Mumtaz, Daniel Hermida-Merino, Eduardo Solano, Didier Cot, Belkacem Tarek Benkhaled, Damien Quemener, Stéphanie Roualdès, Guillaume Fleury, Georges Hadziioannou

# Square Arrays of Vertically Aligned Nanoporous Cylinders from a Linear ABC Triblock Terpolymer

Karim Aissou,[1*] Muhammad Mumtaz,[2] Daniel Hermida-Merino,[3,4] Eduardo Solano,[5] Didier Cot,[1] Belkacem Tarek Benkhaled,[1] Damien Quémener,[1] Stéphanie Roualdes,[1] Guillaume Fleury,[2] and Georges Hadziioannou[2]

[1]Institut Européen des Membranes, IEM, UMR 5635, Univ Montpellier, ENSCM, CNRS, Montpellier, France

[2]Univ. Bordeaux, CNRS, Bordeaux INP, LCPO, UMR 5629, F-33600, Pessac, France

[3]DUBBLE CRG BM26@ESRF, Netherlands Organization for Scientific Research (NWO), 71 Avenue des Martyrs, 38000 Grenoble, France

[4]Departamento de Física Aplicada, CINBIO, Universidade de Vigo, Campus Lagoas-Marcosende, E36310 Vigo, Galicia, Spain

[5]ALBA Synchrotron Light Source, NCD-SWEET Beamline, Cerdanyola del Valles, 08290 Spain

E-mail: karim.aissou@umontpellier.fr

**For Table of Contents use only**

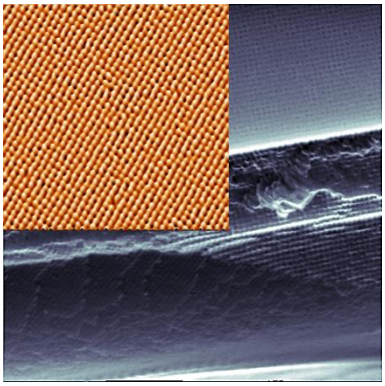

**Abstract:** Vertically oriented nanoporous cylinders, demonstrating an unprecedented alignment persistence, were produced within freestanding poly(1,1-dimethyl silacyclobutane)-*block*-polystyrene-*block*-poly(2-vinyl pyridine) (PDMSB-*b*-PS-*b*-P2VP) layers (~15 $\mu$m thick) blended with short PS-*b*-P2VP chains by combining the non-solvent induced phase separation (NIPS) process with a solvent vapor annealing (SVA) treatment. Here, the NIPS step allowed for the formation of an asymmetric and porous PDMSB-*b*-PS-*b*-P2VP film having a top surface exhibiting poorly-defined nanopores while the subsequent SVA treatment enabled to produce

a symmetric layer that possesses highly-ordered cylindrical nanodomains arranged into a 27 nm period square array. As the unblended NIPS/SVA-made PDMSB-*b*-PS-*b*-P2VP monoliths exhibited a mixed orientation of parallel and perpendicular cylinders, a blending strategy was used to achieve tetragonally-packed PDMSB and P2VP nanodomains having an exceptional vertical alignment persistence. Such solvent-annealed (3h, $CHCl_3$) PDMSB-*b*-PS-*b*-P2VP monoliths blended with 20 wt % of PS-*b*-P2VP chains showed a water permeance close to the value measured through their parent NIPS-made terpolymer films having poorly-ordered nanopores.

**Keywords:** Solvent vapor annealing, block copolymer membrane, self-assembly, vertical alignment, long-range order.

## Introduction

Dense arrays of monodisperse nanodomains having a perpendicular orientation and physical continuity through the entire material thickness are highly-desired in diverse nanotechnology-related applications, including next-generation of electrolytes[1-4] and isoporous membranes.[5-9] For instance, the perfect separation of proteins and viruses having a diameter of tens of nanometers is still challenging, and requires, for a practical use, ultrafiltration (UF) membranes endowed with uniform nanopores in a high areal density.[10] In another example, lithium-ion solid electrolytes have demonstrated an optimized ionic conductivity when the ion conductive nanochannels are aligned perpendicularly to the current-supplying electrodes.[11-13]

Among the different solutions to manufacture materials with large area of vertically aligned monodisperse nanodomains at low cost, the block copolymer (BCP) self-assembly route is one of the most promising approach. Indeed, highly-ordered dense arrays of uniform cylinders having an unidirectional alignment have been achieved in thin film configuration (<1 $\mu$m) by using different methodologies such as equalization of surface energies,[14,15] rough

surfaces,[15-18] top coating,[19,20] solvent vapor annealing (SVA)[21-24] and blending strategy.[25] For instance, Guliyeva *et al*. have produced tetragonally-packed cylinders with a perpendicular orientation from blended ABC-type BCP thin films exposed to a solvent vapor.[26]

To facilitate the implementation of the BCP solution, especially in membrane and solid electrolyte applications, the fabrication of several micrometers thick (freestanding) polymeric films is required in order to reach sufficiently good mechanical properties. However, cylinder-forming BCP films in thick film configuration (>1 $\mu$m) often exhibit cylindrical domains with a mixed orientation (*i.e*., horizontal and perpendicular), making that the ability to generate vertically aligned nanodomains in materials of arbitrary thickness remains difficult to manage with the approaches mentioned above. To overcome this issue, the Osuji group has recently used an interesting electrospray deposition methodology to remarkably produce vertically aligned non-porous polystyrene (PS) cylinders with physical continuity in 4 $\mu$m thick polystyrene-*block*-poly(ethylene-*random*-butylene)-*block*-polystyrene (SEBS) films.[27] Even more striking, Sakurai and coworkers have observed a spontaneous perpendicular orientation of PS cylinders through the directional coalescence of spheres within 15 $\mu$m thick SEBS films.[28]

Here, we use a process that combines a solvent annealing step with a blending strategy to demonstrate a fully perpendicular orientation of nanoporous cylinders within 15 $\mu$m thick terpolymer films. This approach applied to a solvent-annealed poly(1,1-dimethyl silacyclobutane)-*b*-PS-*b*-poly(2-vinyl pyridine) (PDMSB-*b*-PS-*b*-P2VP) layers blended with PS-*b*-P2VP chains enabled the formation of tetragonally-packed cylinders having an exceptional vertical alignment persistence. The physical continuity of highly-ordered nanoporous P2VP domains through the entire film thickness was also confirmed by water permeability measurements. We envision that this particular methodology, enabling the production of vertically oriented nanocylinders with an unprecedented alignment persistence, can provide guidance for the manufacture of novel isoporous freestanding BCP materials.

**Results**

The linear ABC triblock terpolymer used in this work consists of PDMSB (6.7 kg.mol$^{-1}$, $\phi_{PDMSB}$ ~ 0.15), PS (37.3 kg.mol$^{-1}$, $\phi_{PS}$ ~ 0.70) and P2VP (8.5 kg.mol$^{-1}$, $\phi_{P2VP}$ ~ 0.15), where $\phi$ is the volume fraction of the corresponding block. The synchrotron SAXS profile presented in **Figure S1** indicates that the low disperse PDMSB-*b*-PS-*b*-P2VP chains ($Đ$ ~1.06) are arranged into an alternating cylindrical structure having a tetragonal-packing in bulk. Indeed, the scattering peaks follow the ratio of $q/q^* = 1:2^{1/2}:4^{1/2}:5^{1/2}:10^{1/2}:13^{1/2}$, and are associated with the (10), (11), (20), (21), (31) and (32) diffraction planes, respectively, of a square lattice having a period, *p*, of ~26.7 nm as determined from the first-order peak position ($q^*$= 0.0235 Å$^{-1}$, $p = 2\pi/q^*$). Bulk self-assembly of non-frustrated linear ABC triblock terpolymers, that are geometrically symmetric (*i*.e. $\phi_A = \phi_C$) with equivalent surface energies between the A/B and B/C interfaces (*i.e.* $\chi_{AB} \approx \chi_{BC}$ where $\chi$ represents the Flory-Huggins interaction parameter), has been reported in the literature. [29-31] For instance, Mogi *et al*. have demonstrated that a tetragonally-packed cylindrical structure is formed in bulk from various polyisoprene-*b*-PS-*b*-P2VP (PI-*b*-PS-*b*-P2VP) terpolymers having their PS mid-block volume fraction, $\phi_{PS}$, in the ranges of $0.68 < \phi_{PS} < 0.76$.[29] This result is in accordance with the phase behavior of the non-frustrated and geometrically symmetric PDMSB-*b*-PS-*b*-P2VP system studied in this work ($\phi_{PS}$ ~ 0.70). Note that the tetragonally-packed alternating cylindrical structure was theoretically predicted by Phan and Fredrickson as the most stable phase for linear ABC-type BCP chains in the strong segregation limit (SSL).[32] Using the self-consistent field theory (SCFT) in the moderately to strongly segregated regimes, Matsen also confirmed that the tetragonal packing yields a lower free energy than the hexagonal one commonly observed within self-assembled AB-type BCP systems.[33]

**Figure 1a** illustrates the NIPS-SVA process route used to produce vertically oriented cylinders through the entire film thickness. For that purpose, a square shaped PDMSB-*b*-PS-*b*-

P2VP film blended with 20 wt. % of PS-*b*-P2VP chains was first drawn onto a (3 x 3 cm) silicon substrate by using a simple tape casting technique with 250$\mu$m gap from a 18 % wt. terpolymer solution in a di-solvent mixture (DOX/THF: 80/20 by weight) (**1**). To generate an asymmetric terpolymer thick film by NIPS, the solvents were allowed to evaporate during 45s at room temperature (RT) to form a (dark blue) dense air surface layer with a kinetically trapped nanoporous structure (**2**). The blended PDMSB-*b*-PS-*b*-P2VP material was subsequently immersed into a deionized water bath at RT for 5 min to produce a (blue) sponge-like substructure (**3**). Cylinders with an out-of-plane orientation were finally formed within the PDMSB-*b*-PS-*b*-P2VP film by using a SVA treatment (3h, $CHCl_3$) (**4**). The AFM topographic images displayed in **Figure 1b** indicate that the top surface of the blended PDMSB-*b*-PS-*b*-P2VP film generated by NIPS exhibits a poorly-defined phase-separated structure. Conversely, the AFM topographic views presented in **Figure 1c** show that a highly-ordered structure is produced on the film top surface after the SVA treatment. Indeed, after using a low energy CF4 plasma to improve the contrast between the "three-colored" domains (*i.e.*, by preferentially etching PDMSB chains), the pattern consists of a PS matrix separating an alternation of PDMSB (dark) and P2VP (bright) nanodomains arranged into a square array. Note that the 27 nm period square array presented in **Figure 1c**, having a single grain orientation over an area of 2 $\mu m^2$, does not exhibit voided domains after the plasma treatment since the etched depth of PDMSB cylinders was only a few nanometers under the plasma conditions used (45 W, 75 mTorr $CF_4$, and 90s).

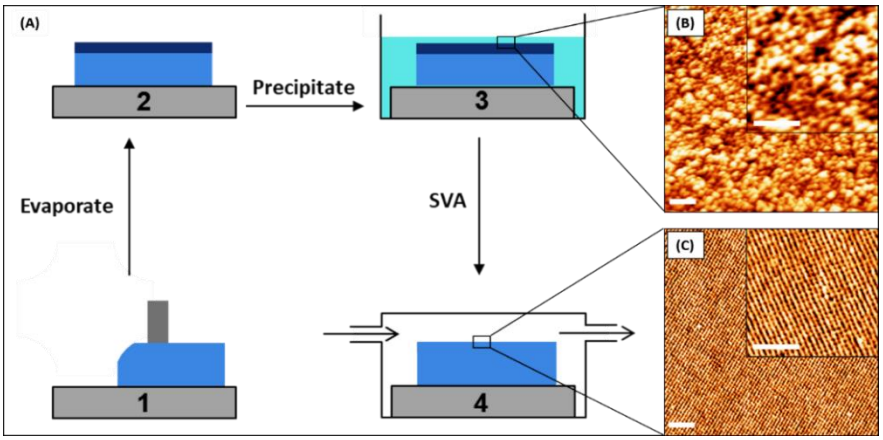


**Figure 1**: (a) Schematic illustration of the NIPS-SVA process route used to produce vertical cylinders with an exceptional alignment persistence. (b) and (c) AFM topographic images showing the film top surface before and after the SVA treatment, respectively. The poorly-defined phase-separated structure generated by NIPS is transformed into a highly-ordered structure having large grains of tetragonally-packed and vertically aligned cylinders. Samples were treated by a low energy $CF_4$ plasma prior AFM imaging to remove the PDMSB top layer and enhance the contrast between the "three-colored" domains so that the PS matrix can be distinguished from the PDMSB and P2VP domains appearing in dark and bright, respectively. Insets: Magnified AFM topographic views confirming the formation of a poorly-defined phase by NIPS and showing more clearly the (dark) PDMSB and (bright) P2VP nanodomains. Scale bars: 250 nm.

**Figure S2** shows a (3 x 3 cm) freestanding NIPS-based PDMSB-*b*-PS-*b*-P2VP/PS-*b*-P2VP film having a thickness of about 21 $\mu$m. To know more about the free surface morphology and gain insight into the porosity within the blended PDMSB-*b*-PS-*b*-P2VP films generated by NIPS, SEM images were also acquired (see **Fig. S3**). The SEM images presented in **Figure S3a-b** show that a poorly defined nanostructure with polydisperse pore sizes is produced on the film top surface while a microporous substructure having large pores can be observed within the terpolymer layer (see **Fig. S3b**). These results indicate the NIPS process allows generating an asymmetric terpolymer film with a highly porous substructure that can be useful for membrane and solid electrolyte applications. However, more often than not, monodisperse nanopores are preferred on the material top surface for nanotechnological applications involving a high selectivity (*i.e.*, a sharp cutoff),[34,35] which is not the case of the kinetically trapped phase generated by NIPS.

To achieve monodisperse nanopores, the top surface morphology of the terpolymer material was reconstructed by using a SVA treatment. Although the NIPS-SVA method requires an additional step to produce isoporous BCP materials compared to the appealing SNIPS (self-assembly + NIPS) process, this methodology does not require extensive optimization to manufacture novel nanostructured membranes, due to complex interplay of influencing parameters inherent to SNIPS, such as solvent composition, polymer molecular weight, casting solution concentration, and evaporation time.[36] In other words, the NIPS-SVA process is a unique method to produce monodisperse nanopores (at equilibrium) when the NIPS methodology cannot be easily applied on a specific BCP system to generate an asymmetric membrane with a skin layer endowed with a well-defined (kinetically trapped) nanostructure.

Because vertically aligned nanochannels are essential in the fabrication of both membranes and electrolytes, a blending strategy has been used to adjust the domain orientation. The SEM images presented in **Figures 2a** and **S4** show that solvent-annealed (3h, $CHCl_3$) PDMSB-*b*-PS-*b*-P2VP films doped with 20 wt. % of PS-*b*-P2VP chains (20 $kg.mol^{-1}$, $\phi_{PS} \sim 0.52$) exhibit vertically oriented PDMSB and P2VP cylinders arranged into a highly-ordered square array having a period of ~27 nm. The magnified SEM view presented in **Figures 2b** allows visualizing different plane cuts of the cylindrical phase in the very close region of the film free surface while the cylinder long axes can be clearly seen from the SEM image displayed in **Figures 2c**.

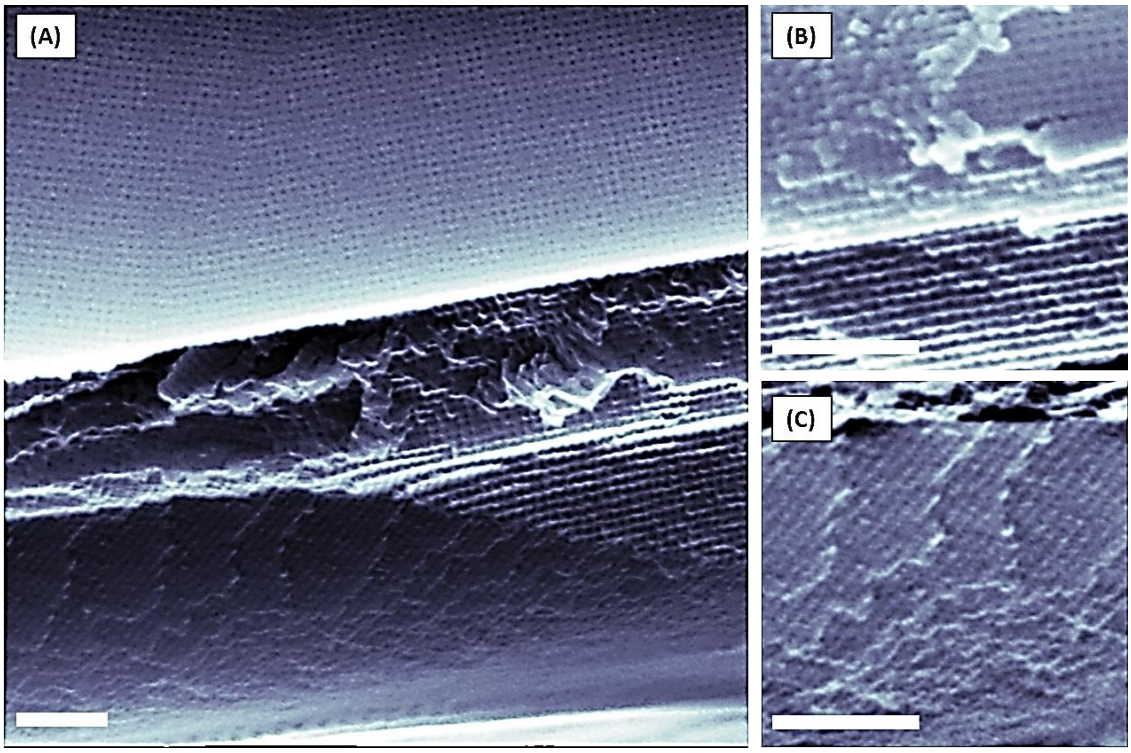


**Figure 2**: (a) Top view SEM image showing of a 27 nm period square array of vertically aligned cylinders formed on the top surface of a PDMSB-*b*-PS-*b*-P2VP/PS-*b*-P2VP film generated by NIPS-SVA (3h, $CHCl_3$) and then treated by a $CF_4$ plasma. (b) and (c) Magnified top view SEM images showing different plane cuts of the tetragonally-packed cylinders and their long axes, respectively. Scale bars: 250 nm.

To further confirm that the cylindrical nanodomains are essentially vertically oriented, GISAXS measurements were also performed on blended terpolymer films exposed to a chloroform vapor for 3h. The 2D GISAXS pattern presented in **Figure 3a** displays Bragg rods, modulated in intensity along the $q_z$ direction, which evidence an out-of-plane orientation of cylindrical nanodomains through the entire film thickness. Indeed, the critical angle was set at 0.2° to ensure a full penetration of the X-Ray beam in the terpolymer layer since a such angle allows a penetration depth > 15 $\mu$m in a PS-*b*-P2VP-based film at 12 keV.[37] The associated intensity cut along the in-plane $q_y$ direction (integrated around the Yoneda position) shows a first-order Bragg peak, $q^*$, at 0.022 $Å^{-1}$ and four higher order peaks located at $q/q^* = 1, 2^{1/2}, 2, 5^{/2}$ and $8^{1/2}$, which is consistent with an alternating cylindrical phase having vertically oriented PDMSB and P2VP domains arranged into a 27 nm period square array (see **Fig. 3b**).

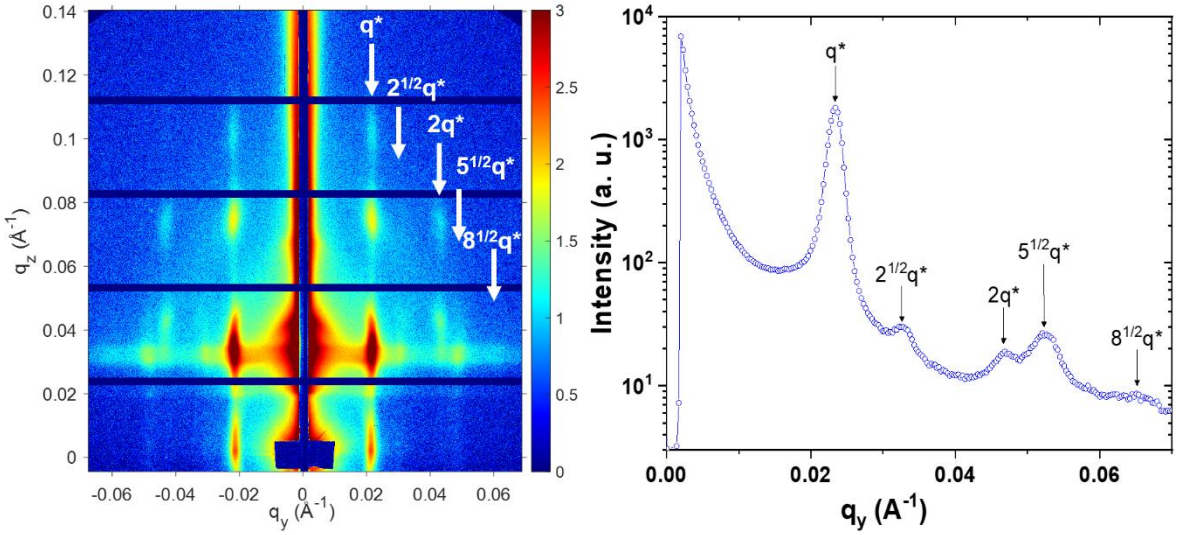


**Figure 3**: (left) 2D GISAXS pattern of a PDMSB-*b*-PS-*b*-P2VP/PS-*b*-P2VP film generated by NIPS-SVA (3h, $CHCl_3$). The incidence angle was set at 0.2°, above the material critical angle, to ensure a full penetration of the X-Ray beam in the terpolymer layer. (right) Associated GISAXS intensity cut along the horizontal $q_y$ direction (taken around the Yoneda band) exhibiting a first-order Bragg peak, $q^*$, at 0.022 $Å^{-1}$ and higher order peaks having relative positions in accordance with a square array of cylinders with a *p*4*mm* symmetry.

The combination of the SVA technique with a homopolymer additive strategy has been already used to achieve a perpendicular domain orientation within the BCP thin films.[25] For instance, the Hillmyer group has demonstrated the formation of vertically oriented nanoporous poly(lactide) (PLA) cylinders over a large thickness window in solvent-annealed PS-*b*-PI-*b*-PS-*b*-PLA thin films blended with 5 wt. % of PLA homopolymer, knowing that a perpendicular alignment of PLA cylinders over a limited range of thicknesses was observed from their unblended homologs.[38] Conversely, the incorporation of AB-type BCP chains to induce an out-of-plane domain orientation is less commonly reported. For example, highly ordered out-of-plane core-shell cylinders were produced on topographically patterned silica substrates regardless of the film thickness by inclusion of 25 wt. % of PDMSB-*b*-PS chains within solvent-annealed (3h, $CHCl_3$) PDMSB-*b*-PS-*b*-poly(methyl methacrylate) (PDMSB-*b*-PS-*b*-PMMA) thin films while their unblended homologs showed a mixed of orientation of parallel and perpendicular core-shell cylinders depending of the terpolymer film thickness.[39]

As we previously demonstrated that the SVA treatments with a long anneal time (> 90 min) can deeply affect the substructure morphology of BCP layers,[40,41] cross-sectional SEM images showing different regions of the blended PDMSB-*b*-PS-*b*-P2VP material manufactured by NIPS-SVA (3h, $CHCl_3$) were also acquired. The cross-sectional views presented in **Figure 4a** show that the 15 $\mu$m thick PDMSB-*b*-PS-*b*-P2VP/PS-*b*-P2VP film has lost its asymmetric and highly-porous architecture generated by NIPS (see **Fig. S3**). Indeed, the blended terpolymer material strongly densified during the SVA treatment to form a symmetric film entirely composed of vertically oriented cylinders that are locally straight (*i.e.*, arranged into a single grain) over several micrometers of the film thickness (see the inset SEM image). The representative SEM images taken in the vicinity of the top and bottom surfaces of the blended PDMSB-*b*-PS-*b*-P2VP monolith, however, suggest that the grain sizes appear larger in the upper region of the material (see **Fig. 4b-c** and **S5**). A decrease of the grain size in the deeper region of the terpolymer film has been recently observed for a perforated-lamellar (PL) phase generated by NIPS-SVA.[40] This phenomenon was explained by the fact that the microporous substructure must densify prior to transform into a well-ordered PL structure, which takes more times in the material lower region due to both the asymmetric architecture of the film generated by NIPS and the solvent accessibility. Here, we speculate that the need to densify the film prior to form the cylindrical nanostructure would further accentuate the development of a grain growth front (at the expense of the sponge-like substructure[40,41]) that is inherent to the formation of a gradient in solvent concentration along the *z*-direction during the SVA treatment.[42,43] This behavior would ultimately favor the formation of anisotropic grains (*i.e.*, larger in the *z*-direction) containing vertically-aligned cylinders, especially when a blending strategy is used.

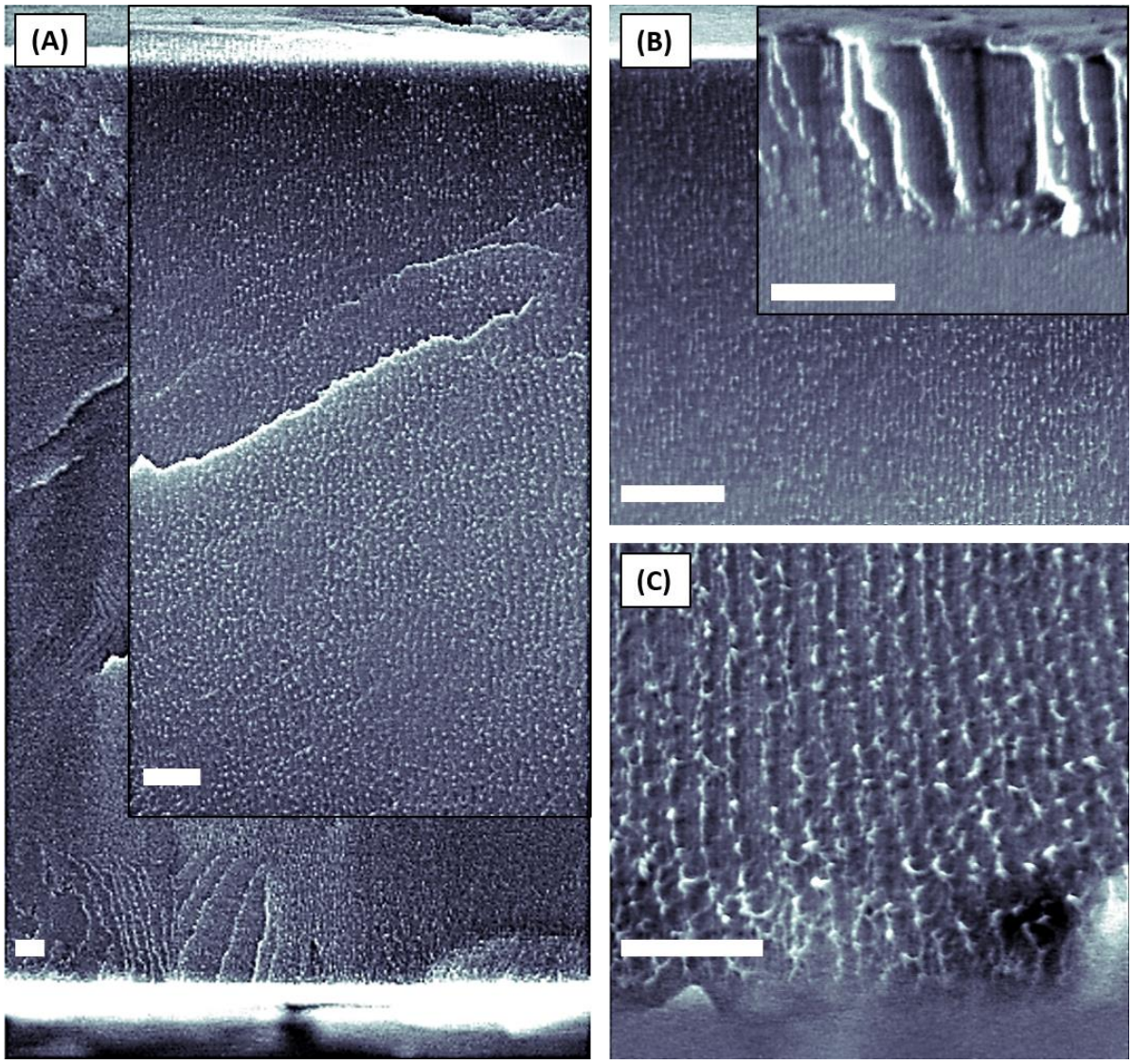


**Figure 4**: Cross-sectional SEM views of a PDMSB-*b*-PS-*b*-P2VP/PS-*b*-P2VP monolith generated by NIPS-SVA (3h, $CHCl_3$) showing (a) the full material having a thickness of ~15 $\mu$m and the presence of vertically oriented cylinders located on the film (b) top and (c) bottom surfaces. Inset: Cross-sectional SEM images showing (a) straight cylinders over 6.5 $\mu$m of the film thickness and (b) a magnified view of cylinders close to the top surface. Scale bars: 500 nm.

As one possible application of monoliths entirely composed of vertically oriented P2VP-based cylinders is their used in membrane technology, flux performance measurements were conducted on both NIPS- and NIPS/SVA-made PDMSB-*b*-PS-*b*-P2VP films blended with 20 wt. % of PS-*b*-P2VP chains. For that purpose, the mean water permeance of three different PDMSB-*b*-PS-*b*-P2VP/PS-*b*-P2VP films exposed to a $CHCl_3$ vapor for 3h has been plotted as a function of the hydraulic pressure applied from 0.5 to 2 bar, using a dead-end stirred

ultrafiltration cell, and was compared to the mean value obtained from the as-cast (no SVA) material (see **Fig. 5**). Regardless of the SVA treatment duration, all blended PDMSB-*b*-PS-*b*-P2VP films deposited on a porous (0.1 $\mu$m) hydrophilic PVDF support demonstrated an excellent stability over material failure even at 2 bar since a linear change in water flux with the increase in pressure drop is observed (water conditions: pH = 7 and T = 22°C). We also observed that the highly porous (asymmetric) terpolymer films generated by NIPS showed a mean water permeance value of 156 L $h^{-1}$ $m^{-2}$ $bar^{-1}$, which is in the same range than the mean value measured from denser (symmetric) materials generated by NIPS-SVA (114 L $h^{-1}$ $m^{-2}$ $bar^{-1}$).

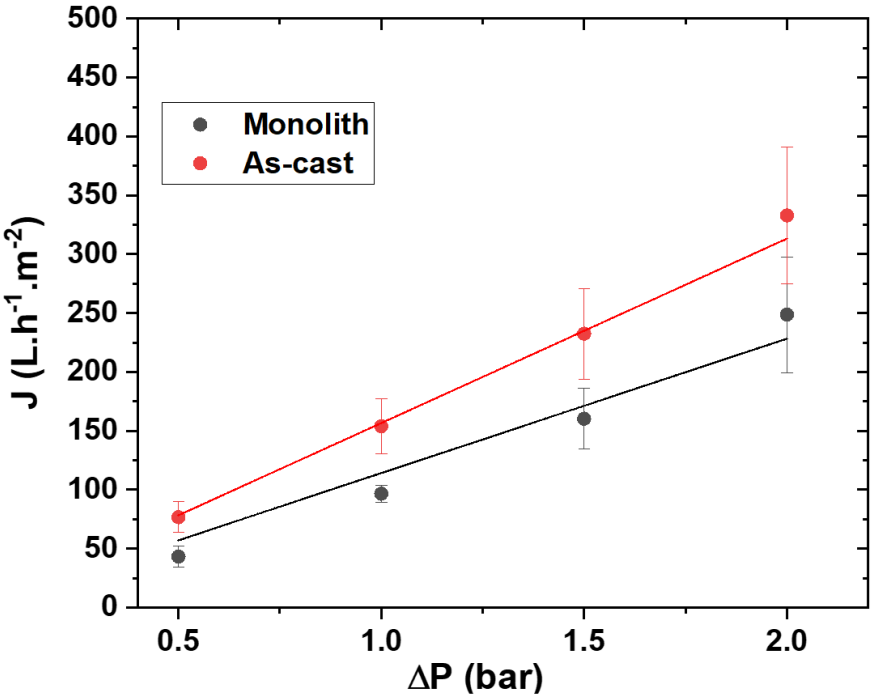


**Figure 5**: Water fluxes, *J*, of the NIPS made PDMSB-*b*-PS-*b*-P2VP/PS-*b*-P2VP materials exposed to a $CHCl_3$ vapor for different times: (red dots) 0 min (only NIPS) and (black dots) 180 min (NIPS-SVA). Error bars are the standard deviations of the mean relative permeability values calculated for 3 different samples.

It is quite surprising to notice that the (as-cast) asymmetric film feebly outperform the solvent-annealed (3h, $CHCl_3$) 15 $\mu$m thick monolithic material since the former exhibits a high porosity as revealed by the SEM images presented in **Figure S3**. This unexpectedly low permeability

might be due the formation of a poor connectivity between the pores during the NIPS process, resulting in the creation of some dead-end pores. At the opposite, the PDMSB-*b*-PS-*b*-P2VP/PS-b-P2VP monoliths, having vertical cylinders with a long range order, show a higher permeability than that reported in the literature from PI-*b*-PS-*b*-P4VP membranes, comprising a sponge-like substructure and a 100 nm thick top surface with P4VP porous domains packed in a 26 nm period square lattice (~24 L $m^{-2}$ $h^{-1}$ $bar^{-1}$).[44] For these PI-*b*-PS-*b*-P4VP membranes, the Wiesner group determined that the calculated permeability (310 L $m^{-2}$ $h^{-1}$ $bar^{-1}$) using the Hagen-Poiseuille (H-P) law (discussed below) is greater than the measured permeability which suggests that the sponge-like substructure contributes to permeability. In other words, the hydraulic pathways formed in their asymmetric substructure are not fully effective like those generated by NIPS within our PDMSB-*b*-PS-*b*-P2VP/PS-b-P2VP films, notably in the absence of a pore-forming agent such as P4VP homopolymer.[35] To extend the comparison, it is worth noting that the hydraulic permeability value measured from an unblended PDMSB-*b*-PS-*b*-P2VP film generated by NIPS-SVA (3h, $CHCl_3$) was found to be very low (~2 L $m^{-2}$ $h^{-1}$ $bar^{-1}$) (see **Fig. S6**). This behavior is due to fact that in-plane (*i.e.*, dead-end) cylinders are mainly formed within the unblended terpolymer material (see **Fig. S7** and **S8**). This result also implicitly confirms that perpendicular cylinders are produced within the blended PDMSB-*b*-PS-*b*-P2VP films generated by NIPS-SVA (3h, $CHCl_3$).

As the NIPS/SVA-treated material exhibits monodisperse cylindrical nanochannels with a fully perpendicular orientation, we attempted to estimate the P2VP pore radius ($R_{P2VP}$) according to the Hagen-Poiseuille law:

$$J = N\frac{\pi\, d^4 \Delta P}{128 \times \mu \times \tau \times L}$$

where $J$ is the flux, $N$ is the areal density of pores ($1.36 \times 10^{15}$ pores/$m^2$), $d$ is the pore diameter, $\Delta P$ is the transmembrane pressure, $\mu$ is the viscosity of water ($9.54 \times 10^{-4}$ Pa.s at 22°C), $\tau$ is the pore tortuosity ($\tau = 1$ for vertically aligned cylinders) and $L$ represents the nanochannel

length. In our case, a permeability, $J/\Delta P$, of 114 L $m^{-2}$ $h^{-1}$ $bar^{-1}$ was measured which gives a P2VP pore radius value of ~9.5 nm, assuming that the hydrophobic PDMSB domains are not permeable to water. This value remains consistent with the lattice constant ($a$ = 27 nm), and is in fairly good agreement with the one extracted from the AFM image ($R_{P2VP,AFM} \approx 8.4$ nm) presented in **Figure S9** from which a PDMSB domain radius of ~6.6 nm was also measured. Note that the P2VP domains are found slightly larger than the PDMSB ones in accordance with the different volume fractions of the terpolymer films blended with 20 wt. % of PS-*b*-P2VP chains ($\phi_{PDMDB} \approx 0.14$, $\phi_{PS} \approx 0.68$ and $\phi_{P2VP} \approx 0.18$).

To know more about the selectivity of PDMSB-*b*-PS-*b*-P2VP/PS-*b*-P2VP monoliths generated by NIPS-SVA (3h, $CHCl_3$), the rejection tests of commercial 20 nm and 40 nm (diameter) gold nanoparticles (NPs) were conducted (see **Fig. 6**). In this regard, UV-visible spectroscopy measurements were performed to determine the Au NP concentrations in the feed and permeate solutions, and the absorbance data were used to calculate the rejection percentage, $R$, as follows:[45]

$$R = (1 - \frac{A_p}{A_f}) \times 100$$

where $A_f$ and $A_p$ are the UV-visible maximum absorbance values of the feed and permeate solutions, respectively.

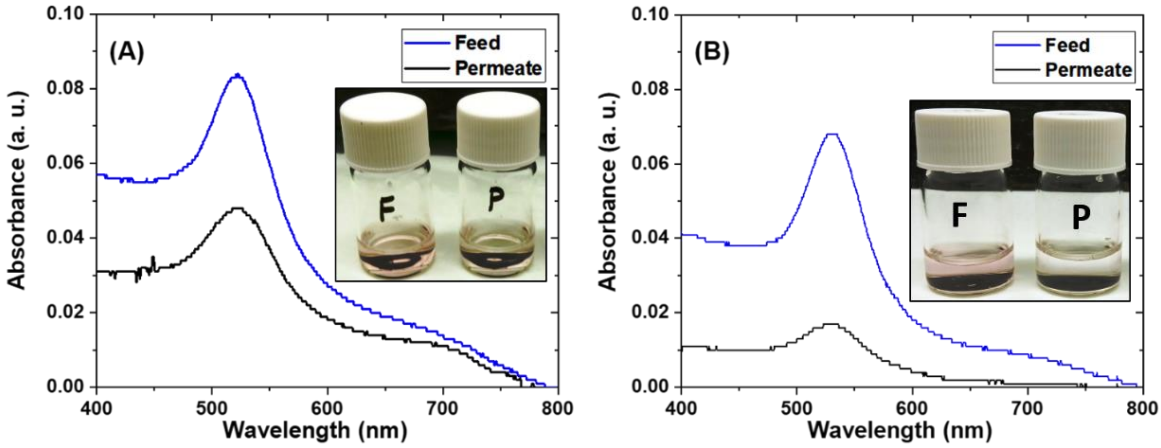


**Figure 6**: (a) and (b) UV-visible spectra of the feed (blue) and permeate (black) recorded over the 400-800 nm spectral range for the 20 nm and 40 nm gold NPs, respectively. All the UV-visible spectra mainly consists of a peak centered at approximately 520 nm (530 nm) that corresponds to the surface plasmon polariton generated by the 20 nm (40 nm) gold NPs. Inset: Photographs showing the (left) feed and (right) permeate solutions.

A rejection of ~43% of 20 nm NPs was achieved at 0.5 bar from the solvent-annealed (3h, $CHCl_3$) PDMSB-*b*-PS-*b*-P2VP/PS-*b*-P2VP monolith (see **Fig. 6a**). This behavior is in accordance with the Gaussian distribution showing a mean radius value of P2VP domains centered on ~8.4 nm (see **Fig. S9b**) and confirms that the water transport is not dominated by the formation of macro defects (> 100 nm) within the blended terpolymer membrane during the SVA process. Interestingly, although the permeate appears colorless in the photograph presented in **Figure 6b**, the 40 nm gold NPs were not completely blocked as expected since a rejection of ~75% was demonstrated at 0.5 bar from the blended PDMSB-*b*-PS-*b*-P2VP monolith generated by NIPS/SVA. To elucidate this phenomenon, dynamic light scattering (DLS) were performed on the feed, permeate and retentate solutions, and it was observed that the average hydrodynamic diameter of Au NPs contained in the permeate solution was ~31 nm while average sizes of ~40 nm and ~43 nm were determined in the feed and retentate solutions, respectively (see **Fig. S10**). Although these results clearly show that only the smaller gold NPs, initially contained in the feed solution, were not blocked by the P2VP pores during the filtration, some defects with a diameter > 30 nm were necessary formed within the blended PDMSB-*b*-

PS-*b*-P2VP monolith, and would explain why the P2VP pore radius determined by the H-P law ($R_{H\text{-}P}$ ~ 9.5 nm) is slightly larger than that measured by AFM ($R_{AFM}$ ~ 8.4 nm).

## Conclusion

We have demonstrated the fabrication of freestanding nanoporous terpolymer monoliths (~15 $\mu$m thick) entirely composed of tetragonally-packed and vertically oriented cylinders. A fully perpendicular orientation of nanoporous nanodomains was achieved by combining a blending strategy with a NIPS-SVA process. This perpendicular orientation of cylinders was demonstrated by direct microscopy (SEM and AFM) and indirect scattering (GISAXS) methods while their physical continuity through the entire film was confirmed by water permeability tests. Such freestanding nanostructured monoliths endowed with vertically aligned monodisperse pores are expected to find applications in advanced membrane and electrolyte technologies.

## Experimental

**Material:** The PDMSB-*b*-PS-*b*-P2VP chains were prepared by anionic polymerization *via* a sequential addition of 1,1-dimethylsilacyclobutane (DMSB), styrene (S) and 2-vinylpyridine (2VP) monomers in THF/heptane (1:1,v/v) solvent mixture at -48°C using *sec*-Butyllithium (*sec*-BuLi) as initiator (**scheme S1**).The reaction was terminated using degassed methanol (MeOH) and the PDMSB-*b*-PS-*b*-P2VP chains were precipitated twice in MeOH prior to be dried in oven at 45°C for overnight. The PDMSB-*b*-PS-*b*-P2VP terpolymer has a molecular weight, $M_n$, of 52 kg mol$^{-1}$ ($Đ$ ~ 1.06) and volume fraction ratios of PDMSB/PS/P2VP = 15:70:15. The PS-*b*-P2VP chains were synthetized by anionic polymerization as described previously[46] to achieve $M_n$ and $\phi_{PS}$ of 20 kg.mol$^{-1}$ ($Đ$ ~ 1.1) and 0.52, respectively. The 20 nm and 40 nm gold NPs, used for the rejection tests, were purchased from Sigma Aldrich.

**Fabrication of asymmetric PDMSB-*b*-PS-*b*-P2VP thick films by NIPS:** Unblended and blended asymmetric PDMSB-*b*-PS-*b*-P2VP films were generated by NIPS following the procedure described in **Figure 1** (steps 1-3). To perform the water permeability tests, some NIPS-based PDMSB-*b*-PS-*b*-P2VP films were deposited on a 100 nm thick poly(3,4-ethylenedioxythiophene) polystyrene sulfonate (PEDOT:PSS, Sigma Aldrich, 2.8% wt. in water) layer in order to facilitate the removal of the terpolymer layer from the substrate. In this case, silicon pieces were treated by an oxygen plasma in a home-made chamber (plasma conditions: 45 W, 75 mTorr $O_2$, 10 min) prior the deposition of the sacrificial PEDOT:PSS layer (spin-coat conditions: speed = 1000 rpm, acceleration = 500 rpm.s$^{-1}$, time = 90s).

**Fabrication of nanostructured PDMSB-*b*-PS-*b*-P2VP monoliths by SVA:** To produce monoliths entirely composed of a cylindrical phase, unblended and blended PDMSB-*b*-PS-*b*-P2VP films generated by NIPS were exposed to a $CHCl_3$ vapor for 3h as shown in **Figure 1** (step 4). Here, a continuous flow system was used to control the $CHCl_3$ vapor pressure (32 sccm $CHCl_3$ + 8 sccm $N_2$) in the SVA chamber as described previously.[47] Note that the PDMSB-*b*-PS-*b*-P2VP films were blended with 20 wt % of PS-*b*-P2VP chains to achieve vertically aligned cylinders while a higher doping level of PS-*b*-P2VP chains (*e.g.*, 30 wt %) within the terpolymer layer resulted in the formation of unidentified phase having hexagonally-packed nanodomains (see **Fig. S11**). Besides, although a residual Debye-Scherrer ring could be observed on the 2D-GISAXS pattern, perpendicular cylinders arranged into a square array were also mainly produced within solvent-annealed (3h, $CHCl_3$) PDMSB-*b*-PS-*b*-P2VP/PS-*b*-P2VP films spin-coated from a 18 % wt. terpolymer solution in a di-solvent mixture (DOX/THF: 80/20 by weight) (see **Fig. S12**). The morphology of vertically-aligned cylinders generated by spin coated-SVA is shown in **Figure S13**. Interestingly, the 2D-GISAXS pattern presented in **Figure S12a** showed a Debye-Scherrer ring consistent with the presence of randomly oriented

nanofeatures having a period of ~31.4 nm within the as-cast (spin-coated) blended terpolymer film.

**AFM and SEM imaging:** Atomic force microscopy (AFM Nano-Observer, CSInstruments) was used in tapping mode to characterize the surface morphology of PDMSB-*b*-PS-*b*-P2VP thick films. Silicon cantilevers (PPP-NCH, Nanosensors) with a typical tip radius of ~5 nm were used. The resonance frequency of cantilevers was about 235 kHz. Scanning electron microscopy (SEM, Hitachi S-4800) was used at an accelerating voltage of 5 kV to acquire top view and cross-section images of both asymmetric thick films and monoliths. Prior to use the AFM and SEM imaging techniques, PDMSB-*b*-PS-*b*-P2VP thick films were treated with a fluorine based plasma in a home-made chamber to improve the image contrast (plasma conditions: 45 W, 75 mTorr $CF_4$, and 90s).

**SAXS and GISAXS characterizations:** SAXS experiments were performed on the D2AM French-CRG Beamline at the European Synchrotron Radiation Facility (ESRF) in Grenoble, France. A XPAD 2D pixel detector was used for recording the 2D scattering images, and a 2400 mm sample-to-detector distance was chosen. The energy of the X-ray beam was 11 keV. The 2D images were radially averaged around the center of the primary beam to obtain the isotropic SAXS intensity profiles. The scattering pattern from a specimen of silver behenate was used for the calibration of the wavevector scale of the scattering curves. Finally, the data were normalized to the intensity of the incident beam to correct for primary beam intensity fluctuations. GISAXS experiments were performed on the Dutch-Belgian Beamline (DUBBLE) at the European Synchrotron Radiation Facility (ESRF) station BM26B in Grenoble.[48] A monochromatic beam of 12 keV was set using a Si (111) double crystal monochromator. The sample (typical size of 150 $mm^2$) was shone with the X-ray beam with an incidence angle of 0.2º, that was above the critical angle of the polymer, ensuring full penetration of the X-ray beam in the material and hence, analyzing the full volume of the

sample. The 2D scattering patterns were collected with a PILATUS3 S 1 M detector. The scattering vector and the sample to detector distance were calibrated using silver behenate as standard, obtaining a sample-to-detector distance of 7500 mm.

**Water flux performances and gold nanoparticle filtrations:** The water permeability of the different PDMSB-*b*-PS-*b*-P2VP thick films was measured in a 10 mL filtration cell (Amicon 8010 stirred cell) connected to a water reservoir and a compressed air line. The measurements were performed on 2.5 cm diameter PDMSB-*b*-PS-*b*-P2VP material discs supported by a high permeable hydrophilic PVDF material (water permeability of ~ 2900 L $h^{-1}$ $m^{-2}$ $bar^{-1}$)[49] in order to achieve reproducible measurements between 0.5 and 2 bar, notably by avoiding large deformations (and eventually ruptures) of the terpolymer film when the pressure drop is higher than 1.5 bar. The mass of water passing through the stacked materials (permeate) was recorded using a connected balance at regular time intervals for 7 min. Water temperature was maintained at 22°C during the measurements while the error bars were calculated from 3 different samples. In order to avoid a non-linear behavior of the water flux with the increase in pressure drop, a transmembrane pressure of 2.5 bar was systematically applied during 10 min on each terpolymer film prior measurements to determine their permeability performance. An UV-visible spectrometer (Shimadzu, UV-2401 PC) was used to measure the 20 nm and 40 nm nm gold NP concentrations in the feed and permeate solutions by recording the UV-visible spectra over the 400-800 nm spectral range. The hydrodynamic diameter distributions of the gold NPs contained in the feed, permeate and retentate solutions were determined with a DLS instrument (Anton Paar, Litesizer 500) equipped with a 40 mW He-Ne laser operating at 658 nm. Samples were analyzed in quartz cuvettes, and the temperature was set at 25°C.

**Acknowledgements**

This work was performed within the support of the ANR JCJC AFM_Ring project, grant ANR-18-CE09-00xx of the French Agence Nationale de la Recherche. D.H.-M acknowledges the "María Zambrano" contract of the University of Vigo, financed by the Spanish Ministerio de Universidades/33.50.460A.752 and by “European Union NextGenerationEU/PRTR”

**References**

(1) Cheng, S.; Smith, D. M.; Pan, Q.; Wang, S.; Li, C. Y. Anisotropic Ion Transport in Nanostructured Solid Polymer Electrolytes. *RSC Adv.* **2015**, *5*, 48793-48810.

(2) Kambe, Y.; Arges, C.G.; Patel, S.; Stoykovish, M.P.; Nealey, P.F. Ion conduction in microphase-separated block copolymer electrolytes. *Electrochem. Soc. Interface* **2017**, *26*, 61-67.

(3) Park, M. J.; Balsara, N. P. Anisotropic Proton Conduction in Aligned Block Copolymer Electrolyte Membranes at Equilibrium with Humid Air. *Macromolecule*s **2010**, *43*, 292-298.

(4) Ramon-Gimenez, L.; Storz, R.; Haberl, J.; Finkelmann, H.; Hoffmann, A. Anisotropic ionic mobility of lithium salts in lamellar liquid crystalline polymer networks. *Macromol. Rapid Commun*. **2012**, *33*, 386- 391.

(5) Abetz, V. Isoporous Block Copolymer Membranes. *Macromol. Rapid Commun.* **2015**, *36* (1), 10–22.

(6) Nunes, S. P. Block Copolymer Membranes for Aqueous Solution Applications. *Macromolecules* **2016**, *49* (8), 2905–2916. 79.

(7) Yin, J.; Yao, X. P.; Liou, J.-Y.; Sun, W.; Sun, Y.-S.; Wang, Y. Membranes with Highly Ordered Straight Nanopores by Selective Swelling of Fast Perpendicularly Aligned Block Copolymers. *ACS Nano* **2013**, *7*, 9961- 9974.

(8) Hampu, N.; Werber, J. R.; Chan, W. Y.; Feinberg, E. C.; Hillmyer, M. A. Next-generation ultrafiltration membranes enabled by block polymers. *ACS Nano* **2020**, *14*, 16446-16471.

(9) Phillip, W. A.; O’Neill, B.; Rodwogin, M.; Hillmyer, M. A.; Cussler, E. L. Self-Assembled Block Copolymer Thin Films as Water Filtration Membranes. *ACS Appl. Mater. Interfaces* **2010**, *2*, 847– 853.

(10) Qiu, X.; Yu, H.; Karunakaran, M.; Pradeep, N.; Nunes, S. P.; Peinemann, K. V. Selective Separation of Similarly Sized Proteins with Tunable Nanoporous Block Copolymer Membranes. *ACS Nano* **2013**, *7* (1), 768-776.

(11) Li, J.; Kamata, K.; Komura, M.; Yamada, T.; Yoshida, H.; Iyoda, T.Anisotropic Ion Conductivity in Liquid Crystalline Diblock Copolymer Membranes with Perpendicularly Oriented PEO Cylindrical Domains. *Macromolecules* **2007**, *40* (23), 8125.8128

(12) Majewski, P.W.; Gopinadhan, M.; Jang, W.-S.; Lutkenhaus, J.L.; Osuji, C.O. Anisotropic ionic conductivity in block copolymer membranes by magnetic field alignment. *J. Am. Chem. Soc*. **2010**, *132*, 17516-17522.

(13) Aissou, K.; Mumtaz, M.; Usluer, Ö.; Pécastaings, G.; Portale, G.; Fleury, G.; Cloutet, E.; Hadziioannou, G. Anisotropic Lithium Ion Conductivity in Single-Ion Diblock Copolymer Electrolyte Thin Films. *Macromol. Rapid Comm.* **2016,** *37* (3), 221-226.

(14) Huang, E.; Rockford, L.; Russell, T. P.; Hawker, C. J. Nanodomain control in copolymer thin films. *Nature* **1998**, *395*,757-758.

(15) Ryu, D. Y., Shin, K., Drockenmuller, E., Hawker, C. J. & Russel, T. P. A generalized approach to the modifiction of solid surfaces. *Science* **2004**, *308*, 236-238.

(16) Sivaniah, E.; Hayashi, Y.; Matsubara, S.; Kiyono, S.; Hashimoto, T.; Fukunaga, K.; Kramer, E. J.; Mates, T. Symmetric diblock copolymer thin films on rough substrates. kinetics and structure formation in pure block copolymer thin films. *Macromolecule*s **2005**, *38*, 1837-1849.

(17) Park, S.; Lee, D. H.; Xu, J.; Kim, B.; Hong, S. W.; Jeong, U.; Xu, T.; Russell, T. P. Macroscopic 10-Terabit-per-Square-Inch Arrays from Block Copolymers with Lateral Order. *Science* **2009**, *323*, 1030.

(18) Aissou, K.; Shaver, J.; Fleury, G.; Pecastaings, G.; Brochon, C.; Navarro, C.; Grauby, S.; Rampnoux, J.-M.; Dilhaire, S.; Hadziioannou, G. Nanoscale Block Copolymer Ordering Induced by Visible Interferometric Micropatterning: A Route towards Large Scale Block Copolymer 2D Crystals. *Adv. Mater*. **2013**, *25*, 213.

(19) Kim, E.; Kim, W.; Lee, K. H.; Ross, C. A; Son, J. G. A top coat with solvent annealing enables perpendicular orientation of sub-10 nm microdomains in Si-containing block copolymer thin films. *Adv. Funct. Mater.* **2014**, *24*, 6981-6988.

(20) Bates, C. M.; Seshimo, T.; Maher, M. J.; Durand, W. J.; Cushen, J. D.; Dean, L. M.; Blachut, G.; Ellison, C. J.; Willson, C. G. Polarity-Switching Top Coats Enable Orientation of Sub–10-nm Block Copolymer Domains. *Science **2012***, 338, 775-779.

(21) Kim, G.; Libera, M. Morphological Development in Solvent-Cast Polystyrene-Polybutadiene-Polystyrene (SBS) Triblock Copolymer Thin Films. *Macromolecules* **1998**, *31*, 2569-2577.

(22) Kim, S. H.; Misner, M.; Xu, T.; Kimura, M.; Russell, T. P.Highly Oriented and Ordered Arrays from Block Copolymers via Solvent Evaporation. *Adv. Mater*. **2004**, *16*, 226-231.

(23) Son, J. G.; Gotrik, K. W.; Ross, C. A. High-Aspect-Ratio Perpendicular Orientation of PS-*b*-PDMS Thin Films under Solvent Annealing. *ACS Macro Lett.* **201**2, *1*, 1279-1284.

(24) Sinturel, C.; Vayer, M.; Morris, M.; Hillmyer, M. A. Solvent Vapor Annealing of Block Polymer Thin Films. *Macromolecules* **2013**, *46* (14), 5399-5415.

(25) Jeong, U.; Ryu, D. Y.; Kho, D. H.; Kim, J. K.; Goldbach, J. T.; Kim, D. H.; Russell, T. P. Enhancement in the Orientation of the Microdomain in Block Copolymer Thin Films Upon the Addition of Homopolymer. *Adv. Mater.* **2004**, *16*, 533-536.

(26) Guliyeva, A.; Vayer, M.; Warmont, F.; Faugère, A. M.; Andreazza, P.; Takano, A.; Matsushita, Y.; Sinturel, C. Thin Films with Perpendicular Tetragonally Packed Rectangular Rods Obtained from Blends of Linear ABC Block Terpolymers. *ACS Macro Lett.* **2018**, *7*, 789

(27) Hu, H.; Choo, Y.; Feng, X.; Osuji, C. O. Physical Continuity and Vertical Alignment of Block Copolymer Domains by Kinetically Controlled Electrospray Deposition *Macromol. Rapid Commun*. **2015**, 36, 1290.

(28) Sakurai, S.; Bando, H.; Yoshida, H.; Fukuoka, R.; Mouri, M.; Yamamoto, K.; Okamoto, S. Spontaneous perpendicular orientation of cylindrical microdomains in a block copolymer thick film. *Macromolecules* **2009**, *42*, 2115- 2121.

(29) Mogi, Y.; Nomura, M.; Kotsuji, H.; Ohnishi, K.; Matsushita, Y.; Noda, I. Superlattice Structures in Morphologies of the ABC Triblock Copolymers. *Macromolecules* **1994**, *27*, 6755-6760.

(30) Epps, T. H.; Bailey, T. S.; Waletzko, R.; Bates, F. S. Phase Behavior and Block Sequence Effects in Lithium Perchlorate-Doped Poly(isoprene-*b*-styrene-*b*-ethylene oxide) and Poly(styrene-*b*-isoprene-*b*-ethylene oxide) Triblock Copolymers. *Macromolecules* **2003**, *36*, 2873-2881.

(31) Aissou, K.; Mumtaz, M.; Alvarez-Fernandez, A.; Mercat, J.; Antoine, S.; Pécastaings, G.; Ponsinet, V.; Dobrzynski, C.; Fleury, G., Hadziioannou, G. Metallic Nanodot Patterns with Unique Symmetries Templated from ABC Triblock Terpolymer Networks *Macromol. Rapid Commun.* **2018**, *39*, 1700754.

(32) Phan, S.; Fredrickson, G. H. Morphology of symmetric ABC triblock copolymers in the strong segregation limit. *Macromolecules* **1997**, *31*, 59-63.

(33) Matsen, M. W. Gyroid versus double-diamond in ABC triblock copolymer melts. *J. Chem. Phys.* **1998**, *108*, 785-796.

(34) Peinemann, K. V.; Abetz, V.; Simon, P. F. W. Asymmetric Superstructure Formed in a Block Copolymer via Phase Separation. *Nat. Mater.* **2007**, *6* (12), 992-996.

(35) Phillip, W. A.; Mika Dorin, R.; Werner, J.; Hoek, E. M. V.; Wiesner, U.; Elimelech, M. Tuning Structure and Properties of Graded Triblock Terpolymer-Based Mesoporous and Hybrid Films. *Nano Lett.* **2011**, 11 (7), 2892-2900.

(36) Marques, D. S.; Vainio, U.; Chaparro, N. M.; Calo, V. M.; Bezahd, A. R.; Pitera, J. W.; Peinemann, K.-V.; Nunes, S. P. Self-Assembly in Casting Solutions of Block Copolymer Membranes. *Soft Matter* **2013**, 9 (23), 5557.

(37) Saito, I.; Miyazaki, T.; Yamamoto, K. Depth-Resolved Structure Analysis of Cylindrical Microdomain in Block Copolymer Thin Film by Grazing-Incidence Small-Angle X-ray Scattering Utilizing Low-Energy X-rays. *Macromolecules* **2015**, *48*, 8190– 8196.

(38) Jackson, E. A.; Lee, Y.; Radlauer, M. R.; Hillmyer, M. A. Well-Ordered Nanoporous ABA Copolymer Thin Films via Solvent Vapor Annealing, Homopolymer Blending, and Selective Etching of ABAC Tetrablock Terpolymers ACS Appl. Mater. Interfaces **2015**, 7, 27331– 27339.

(39) Aissou, K.; Mumtaz, M.; Marcasuzaa, P.; Brochon, C.; Cloutet, E.; Fleury, G.; Hadziioannou, G. Highly Ordered Nanoring Arrays Formed by Templated Si-Containing Triblock Terpolymer Thin Films. *Small* **2017**, *13*, 1603184.

(40) Aissou, K.; Mumtaz, M.; Bouzit, H.; Pécastaings, G.; Portale, G.; Fleury, G.; Hadziioannou, G. Bicontinuous Network Nanostructure with Tunable Thickness Formed on Asymmetric Triblock Terpolymer Thick Films. *Macromolecules* **2019**, 4413– 4420.

(41) Aissou, K.; Mumtaz, M.; Demazy, N.; Pécastaings, G.; Fleury, G.; Hadziioannou, G. Periodic Bicontinuous Structures Formed on the Top Surface of Asymmetric Triblock Terpolymer Thick Films. *ACS Macro Lett.* **2019**, *8*, 923– 930.

(42) Kim, S. H.; Misner, M. J.; Xu, T.; Kimura, M.; Russell, T. P. Highly oriented and ordered arrays from block copolymers via solvent evaporation. *Adv. Mater.* **2004**, *16* (3), 226.

(43) Berezkin, A. V.; Papadakis, C. M.; Potemkin, I. I. Vertical domain orientation in cylinder-forming diblock copolymer films upon solvent vapor annealing. *Macromolecules* **2016**, *49*, 415– 424.

(44) Dorin, R. M.; Phillip, W. A.; Sai, H.; Werner, J.; Elimelech, M.; Wiesner, U. Designing Block Copolymer Architectures for Targeted Membrane Performance *Polymer* **2014**, *55*, 347– 353.

(45) Valade, D.; Wong, L. K.; Jeon, Y.; Jia, Z.; Monteiro, M. J. Polyacrylamide Hydrogel Membranes with Controlled Pore Sizes. *J. Polym. Sci., Part A: Polym. Chem.* **2013**, *51*, 129−138.

(46) Antoine, S.; Aissou, K.; Mumtaz, M.; Telitel, S.; Pecastaings, G.;́ Wirotius, A.-L.; Brochon, C.; Cloutet, E.; Fleury, G.; Hadziioannou, G. Core−Shell Double Gyroid Structure Formed by Linear ABC Terpolymer Thin Films. *Macromol. Rapid Commun*. **2018**, *39*, 1800043.

(47) Gotrik, K. W.; Hannon, A. F.; Son, J. G.; Keller, B.; Alexander-Katz, A.; Ross, C. A. Morphology Control in Block Copolymer Films Using Mixed Solvent Vapors. *ACS Nano* **2012**, *6* (9), 8052-8059.

(48) Portale, G.; Hermida-Merino, D.; Bras, W. Polymer research and synchrotron radiation perspectives. *Eur. Polym. J.*, **2016**, *81*, 415-432.

(49) Aissou, K.; Bouzit, H.; Krusch, F.; Méricq, J.-P.; Cot, D.; Masquelez, N.; Roualdes, S.; Quémener, D. Asymmetric Solvent-Annealed Triblock Terpolymer Thick Films Topped by a Hexagonal Perforated Lamellar Nanostructure. *Macromol. Rapid Commun.* **2022**, *43* (2), 2100585.